

Dartmouth College Dartmouth Digital Commons

Dartmouth Faculty Open Access Articles

Open Dartmouth: Faculty Open Access

6-4-2015

Field line distribution of mass density at geostationary orbit

Richard Denton
Dartmouth College

Kazue Takahashi
Johns Hopkins University

Jimyoung Lee
Dartmouth College

C.K. Zeitler
Dartmouth College

N.T. Wimer
Dartmouth College

See next page for additional authors

Follow this and additional works at: <http://digitalcommons.dartmouth.edu/facoa>

 Part of the [Geophysics and Seismology Commons](#)

Recommended Citation

Denton, Richard; Takahashi, Kazue; Lee, Jimyoung; Zeitler, C.K.; Wimer, N.T.; Litscher, E.; Singer, H.J.; and Min, Kyungguk, "Field line distribution of mass density at geostationary orbit" (2015). *Dartmouth Faculty Open Access Articles*. 52.
<http://digitalcommons.dartmouth.edu/facoa/52>

This Article is brought to you for free and open access by the Open Dartmouth: Faculty Open Access at Dartmouth Digital Commons. It has been accepted for inclusion in Dartmouth Faculty Open Access Articles by an authorized administrator of Dartmouth Digital Commons. For more information, please contact dartmouthdigitalcommons@groups.dartmouth.edu.

Authors

Richard Denton, Kazue Takahashi, Jimyoung Lee, C.K. Zeitler, N.T. Wimer, E. Litscher, H.J. Singer, and Kyungguk Min

1 **Field Line Distribution of Mass Density at** 2 **Geostationary Orbit**

R. E. Denton¹, Kazue Takahashi², Jimyoung Lee¹, C. K. Zeitler^{1,3},
N. T. Wimer^{1,4}, L. E. Litscher¹, H. J. Singer⁵, and Kyungguk Min⁶

R. E. Denton and Jimyoung Lee, Department of Physics and Astronomy, Dartmouth College, Hanover, NH 03755, USA. (richard.e.denton@dartmouth.edu, jinmyoung.lee.16@dartmouth.edu, lauren.e.litscher.12@alum.dartmouth.org)

Kyungguk Min, 206 Allison Lab, Auburn University, Auburn, AL 36849, USA. (kmin@auburn.edu)

H. J. Singer, NOAA Space Weather Prediction Center, 325 Broadway, Boulder, CO, 80305, USA. (howard.singer@noaa.gov)

K. Takahashi, Johns Hopkins University Applied Physics Laboratory, 11100 Johns Hopkins Rd, Laurel, MD 20723-6099, USA. (kazue.takahashi@jhuapl.edu)

N. T. Wimer, Department of Mechanical Engineering, University of Colorado, Boulder, CO, 80305, USA. (nicholas.wimer@gmail.com)

C. K. Zeitler, Department of Physics, University of Illinois, 1110 West Green Street, Urbana, IL 61801-3080, USA. (Christopher.K.Zeitler.12@alum.dartmouth.org)

¹Department of Physics and Astronomy,

Abstract. The distribution of mass density along the field lines affects the ratios of toroidal (azimuthally oscillating) Alfvén frequencies, and given the ratios of these frequencies we can get information about that distribution. Here we assume the commonly used power law form for the field line distribution, $\rho_m = \rho_{m,eq}(LR_E/R)^\alpha$, where $\rho_{m,eq}$ is the value of the mass density ρ_m at the magnetic equator, L is the L shell, R_E is the Earth's radius, R is the geocentric distance to a point on the field line, and α is the

Dartmouth College, Hanover, New
Hampshire, USA

²Applied Physics Laboratory, Johns
Hopkins University, Laurel, Maryland, USA

³Department of Physics, University of
Illinois, Urbana, Illinois, USA

⁴Department of Mechanical Engineering,
University of Colorado, Boulder, Colorado,
USA

⁵National Oceanic and Atmospheric
Administration Space Weather Prediction
Center, Boulder, Colorado, USA

⁶Department of Physics, Auburn
University, Auburn, Alabama, USA

10 power law coefficient. Positive values of α indicate that ρ_m increases away
11 from the magnetic equator, zero value indicates that ρ_m is constant along
12 the magnetic field line, and negative α indicates that there is a local peak
13 in ρ_m at the magnetic equator. Using 12 years of observations of toroidal Alfvén
14 frequencies by the Geostationary Operational Environmental Satellites (GOES),
15 we study the typical dependence of inferred values of α on the magnetic lo-
16 cal time (MLT), the phase of the solar cycle as specified by the F10.7 extreme
17 ultraviolet solar flux, and geomagnetic activity as specified by the auroral
18 electrojet (AE) index. Over the mostly dayside range of the observations,
19 we find that α decreases with respect to increasing MLT and F10.7, but in-
20 creases with respect to increasing AE. We develop a formula that depends
21 on all three parameters, $\alpha_{3Dmodel} = 2.2 + 1.3 \cdot \cos(\text{MLT} \cdot 15^\circ) + 0.0026 \cdot \text{AE} \cdot$
22 $\cos((\text{MLT} - 0.8) \cdot 15^\circ) + 2.1 \cdot 10^{-5} \cdot \text{AE} \cdot \text{F10.7} - 0.010 \cdot \text{F10.7}$, that models the
23 binned values of α within a standard deviation of 0.3. While we do not yet
24 have a complete theoretical understanding of why α should depend on these
25 parameters in such a way, we do make some observations and speculations
26 about the causes. At least part of the dependence is related to that of $\rho_{m,eq}$;
27 higher α , corresponding to steeper variation with respect to MLAT, occurs
28 when $\rho_{m,eq}$ is lower.

1. Introduction

29 The field line distribution of mass density should have an important effect on many
 30 MHD scale phenomenon. It controls the field line structure of Alfvén waves, which can
 31 make a large difference in the radial diffusion of radiation belt electrons [*Perry et al.*,
 32 2005]. It would definitely alter the degree of focusing of fast mode waves propagating into
 33 the magnetosphere [*Kress et al.*, 2007], and will probably affect the structure of cavity
 34 mode resonances [*Kwon et al.*, 2012, and references therein].

35 The field line distribution of mass density also affects the frequency of toroidal (az-
 36 imuthally oscillating) Alfvén waves. If the frequency of these waves, measured by ground
 37 magnetometers [*Waters et al.*, 2006] or spacecraft [*Denton*, 2006], is used to calculate the
 38 magnetospheric mass density, an incorrect assumption about the field line distribution
 39 can cause an error in the inferred mass density. Since the theoretical frequency of Alfvén
 40 waves f_{th} will be proportional to the equatorial Alfvén speed $\propto 1/\sqrt{\rho_m}$, the equatorial
 41 mass density ρ_m can be found from $f_{\text{obs}}/f_{\text{th}}(1 \text{ amu/cm}^3) = \sqrt{(1 \text{ amu/cm}^3)/\rho_m}$, where f_{obs}
 42 is the observed Alfvén frequency, and $f_{\text{th}}(1 \text{ amu/cm}^3)$ is the theoretical frequency for an
 43 equatorial mass density of 1 amu/cm^3 . This means that there will be an error in the
 44 inferred ρ_m proportional to the error of f_{th}^2 .

The magnitude of such errors can be estimated from the normalized Alfvén frequencies
 calculated by *Schulz* [1996] if we assume the power law field line distribution for ρ_m

$$\rho_m = \rho_{m,eq} \left(\frac{LR_E}{R} \right)^\alpha, \quad (1)$$

45 that has been used by many researchers [*Waters et al.*, 2006; *Denton*, 2006]. Here $\rho_{m,eq}$ is
 46 the value of the mass density ρ_m at the magnetic equator; $L \equiv R_{\text{max}}/R_E$, where R_{max} is the

47 maximum geocentric distance to any point on the field line, and R_E is the Earth's radius;
48 and α is the power law coefficient (Schulz's m). For the purpose of defining L we use the
49 TS05 magnetic field model [Tsyganenko and Sitnov, 2005]. Note that $\alpha = 0$ corresponds
50 to constant ρ_m along the field line, $\alpha > 0$ corresponds to ρ_m that increases with respect to
51 the magnetic latitude, MLAT, toward the ionosphere, and $\alpha < 0$ corresponds to ρ_m that
52 is locally peaked at the magnetic equator. If one includes the part of the field line that
53 approaches the ionosphere, $\alpha > 0$ would seem to be most realistic, but it is the portion
54 of the magnetic field line close to the magnetic equator (where the magnetic field B is
55 small) that often plays a dominant role in determining the Alfvén frequency. So it is
56 possible for $\alpha < 0$ to be relevant, indicating that ρ_m is locally peaked near the magnetic
57 equator, even though ρ_m must eventually increase at large MLAT. In previous calculations
58 using data from the Geostationary Operational Environmental Satellites (GOES), the
59 field line distribution implied by (1) was probably not accurate for $|\text{MLAT}|$ beyond about
60 25° [Takahashi and Denton, 2007].

61 If we use the fundamental mode frequency at geostationary orbit to infer ρ_m and assume
62 that α is equal to 3, but the realistic field line distribution corresponds to $\alpha = 0$, the
63 inferred value of ρ_m will be 15% lower than the actual value. For the purpose of calculating
64 the mass density, it would be useful to reduce even this uncertainty. But the uncertainty
65 increases if a harmonic higher than the fundamental mode is used. If we use the third
66 harmonic to infer ρ_m , the estimated ρ_m becomes 33% lower than the actual value. This
67 error would increase if the mass density is locally peaked at the magnetic equator ($\alpha < 0$).
68 The third harmonic is the most frequently observed toroidal Alfvén wave observed by
69 GOES [Takahashi et al., 2010], so this is an important case.

70 The field line distribution of ρ_m can be estimated based on the ratios of frequencies of the
 71 harmonics of toroidal Alfvén waves [*Takahashi and McPherron, 1982; Price et al., 1999;*
 72 *Takahashi and Denton, 2007; Denton et al., 2006b, 2009*]. The basic idea is fairly simple.
 73 Mass density localized on one part of the field line affects the frequencies of different
 74 harmonics to a different extent. For instance, a peak in ρ_m strongly localized to the
 75 magnetic equator would lower the frequency of the fundamental mode ($n = 1$) and other
 76 odd harmonics, because those modes have a nonzero velocity at the magnetic equator. But
 77 such a steep peak in ρ_m would not lower the frequency of the second harmonic ($n = 2$)
 78 or other even harmonics, because the velocity is zero for those modes at the magnetic
 79 equator. The inertia only affects the mode if there is acceleration at the position of that
 80 inertia. Consequently, if a steep peak in ρ_m is added at the magnetic equator, the ratio
 81 f_2/f_1 will increase. In this paper, the frequency ratios will be normalized to the most
 82 frequently observed third harmonic, so that our normalized frequencies $\bar{f}_n \equiv f_n/f_3$. By
 83 varying α so as to reduce the least squared difference between the observed and theoretical
 84 values of \bar{f}_n , we infer the most appropriate value of α .

85 In principle, if one wants to use toroidal Alfvén frequencies to get ρ_m for a particular
 86 event, one might be able to measure the frequencies of several harmonics and get both $\rho_{m,eq}$
 87 and α . *Denton et al.* [2009] have apparently done this successfully using the frequencies
 88 of toroidal Alfvén waves measured by the Cluster spacecraft. But in most cases, the error
 89 in inferred values of α found for particular events is large [*Takahashi and McPherron,*
 90 *1982; Denton et al., 2001, 2004*] owing to the sensitivity of the toroidal Alfvén frequencies
 91 to the field line distribution [*Denton and Gallagher, 2000*]. For that reason, most of our
 92 recent studies of the field line distribution of ρ_m have been statistical [*Takahashi et al.,*

2004; *Denton et al.*, 2006b; *Takahashi and Denton*, 2007]. Using many observations of
the normalized frequency ratios \bar{f}_n , we can get an accurate measure of at least the typical
field line distribution.

Angerami and Carpenter [1966] presented theoretical field line distributions that can
be approximated by values of α between 0.5 and 1 for diffusive equilibrium (more likely
relevant in the high density plasmasphere [*Takahashi et al.*, 2014, and references therein])
and $\alpha = 4$ for a collisionless equilibrium (possibly relevant for the low density plasma-
trough) [*Takahashi et al.*, 2004]. *Denton et al.* [2006b] did a statistical study of toroidal
Alfvén frequencies measured by the Combined Release and Radiation Effects Satellite
(CRRES), and recommended $\alpha = 1$ for the field line distribution at $L > 5$ if the power
law model was used. This includes times during which the spacecraft might have been
in the plasmasphere or plasmatrrough. They found evidence for a local peak in ρ_m at
the magnetic equator under certain conditions, especially with large geomagnetic activity
(large Kp index or large negative Dst). *Takahashi and Denton* [2007], did a statistical
study using toroidal Alfvén frequencies measured by GOES and found that there was
evidence for a local peak in ρ_m at the magnetic equator in the afternoon magnetic local
time MLT sector, but not in the dawn MLT sector. Studies finding α at lower values of
 L have been summarized by *Denton* [2006].

Here our goal is to develop a model for α that depends on MLT, geomagnetic activity
as indicated by the auroral electrojet (AE) index, and solar radiation as indicated by the
F10.7 index. The value of AE may be related to substorm activity. The value of F10.7
is related to the phase of the solar cycle. Large F10.7 corresponds to solar maximum,
while small F10.7 corresponds to solar minimum. In section 2, we describe the data and

116 method used in the study; in section 3, we describe our modeling results for variation
117 with respect to a single parameter (MLT, F10.7, or AE); in section 4, we describe our
118 modeling results with simultaneous variation of all three parameters; and in section 5 we
119 discuss these results.

2. Data and Method

120 The database of toroidal (azimuthally oscillating) Alfvén wave frequencies that we will
121 use has been described by *Takahashi et al.* [2010]. Frequencies were obtained from mag-
122 netometer data on five Geostationary Operational Environmental Satellites (GOES) over
123 a 12 year period from 1980 to 1991. The data was scanned in 30 min time windows that
124 moved forward in 10 min steps. The maximum entropy method (MEM) [*Press et al.*,
125 1986] was used to find peaks in the power spectra, and an interactive method was used to
126 identify most of the third harmonic ($n = 3$) frequencies. Using the algorithm below, some
127 additional third harmonic frequencies were identified automatically because their frequen-
128 cies and times of observation were close to those of manually identified third harmonic
129 frequencies.

130 Whereas *Takahashi et al.* [2010] used only the most commonly observed third harmonic
131 ($n = 3$), we will make use of harmonics up to $n = 4$. In order to determine the harmonic
132 number, we normalize all the frequencies to third harmonic frequencies. In order to
133 normalize a frequency observed at time t , a third harmonic frequency had to be identified
134 within 10 min of t . Considering the 10 min resolution of our data, this means that a
135 third harmonic frequency had to be identified either at the time of observation or one
136 time step earlier or later. If a third harmonic frequency was identified on one side of an
137 observation and another third harmonic frequency was identified within 20 min on the

138 other side of the observation, we interpolated the two third harmonic frequencies to the
 139 time of observation. With the observed frequency f and the nearby or interpolated third
 140 harmonic frequency f_3 , we calculate the normalized frequency $\bar{f} \equiv f/f_3$.

Since we are normalizing to the third harmonic frequencies, we discarded the normalized
 third harmonic frequencies (equal to unity). We further limited the data in several ways.
 We discarded normalized frequencies above 1.5; these values occur for harmonics over
 $n = 4$. For each harmonic number n , we calculated the uncertainty of the normalized
 frequency $\delta\bar{f}_n$, using

$$\delta\bar{f}_n = \bar{f}_n \sqrt{\left(\frac{\delta f_n}{f_n}\right)^2 + \left(\frac{\delta f_3}{f_3}\right)^2}, \quad (2)$$

141 and discarded the resulting normalized frequencies for which the uncertainty was greater
 142 than 0.1. And we further limited the data to time periods for which the AE index was
 143 available. This eliminated most of the one and a half year period between the midpoint
 144 of 1988 and the beginning of 1990. While the frequency ratios of the Alfvén waves varied
 145 with geomagnetic activity based on the Kp index, the Dst index, and the AE index, we
 146 found that there was a somewhat greater dependence on AE than on the other indices
 147 (not shown). Therefore we decided to use the AE index as a measure of geomagnetic
 148 activity. After these reductions, we still had 211,808 normalized frequencies.

Figure 1 shows the distribution of normalized frequencies \bar{f} used in our study. With
 these frequencies, we will examine the statistical variation of the field line distribution.
 Here, we solve for Alfvén wave eigenmodes using the procedure of *Denton et al.* [2006b].
 We use the *Singer et al.* [1981] wave equation with the power law form (1) for the field
 line distribution of mass density and with a dipole magnetic field at $L = 6.8$, a nominal
 equatorial distance for GOES spacecraft. For the entire set of times of our frequency

measurements, the mean L value was 6.8 with a standard deviation of 0.13. Note that *Takahashi et al.* [2004] found, for the purpose of determining the field line distribution, that the use of a different magnetic field model did not significantly alter the results. We assume that there is a perfectly conducting boundary at an altitude of 100 km. Then we start with a guess for the power law coefficient α and vary α and $\rho_{m,eq}$ (at each value of α) to find the best fit between the observed and calculated frequency ratios \bar{f} by minimizing the quantity

$$S \equiv \sum_{n=1\dots 4} w_n \left(\bar{f}_{\text{obs},n} - f_{\text{th},n} \right)^2, \quad (3)$$

149 where for each harmonic n , the weight $w_n = 1/(\delta \bar{f}_{\text{obs},n})^2$, $\delta \bar{f}_{\text{obs},n}$ is the uncertainty in the
 150 observed normalized frequency $\bar{f}_{\text{obs},n}$, and $f_{\text{th},n}$ is the theoretical frequency. While $\bar{f}_{\text{obs},3}$ is
 151 unity, $f_{\text{th},3}$ is an unnormalized frequency (dependent on $\rho_{m,eq}$), and is only approximately
 152 equal to unity (because of the minimization with respect to $\rho_{m,eq}$). The solution leads
 153 to best fit values for both $\rho_{m,eq}$ and α , but the value of $\rho_{m,eq}$ is meaningless because the
 154 observed frequencies were rescaled (normalized to $f_{\text{obs},n}$). Note that variation in $\rho_{m,eq}$
 155 merely changes all the frequencies $f_{\text{th},n}$ by a common factor. Here we are only interested
 156 in the values of α .

157 For $n = 3$, we used the weight $w_3 = \sum_{n=1,2,4} (\bar{f}_{\text{obs},n} / \delta \bar{f}_{\text{obs},n})^2$. This formula is motivated
 158 by the idea that we could work backwards to get the third harmonic frequency from the
 159 other harmonics. We assume that the uncertainty for f_3 based on another harmonic is
 160 equal to the relative error of that harmonic. The absolute error would be unity times that
 161 relative error, and the separate weights add in quadrature assuming that they are inde-
 162 pendent measurements [*Lyons*, 1991]. We tested this method with sets of data including
 163 random errors and it yielded a more accurate and precise result than the other methods

164 we tried (including normalizing the theoretical frequencies to $f_{\text{th},3}$ and fitting $\bar{f}_{\text{obs},n}$ to
 165 $\bar{f}_{\text{th},n}$ for only $n = 1, 2,$ and 4).

166 For instance, fitting Gaussians to the three peaks in Figure 1, we find $\bar{f}_1 \equiv f_1/f_3 =$
 167 $0.236 \pm 0.034,$ $\bar{f}_2 = 0.638 \pm 0.037,$ and $\bar{f}_4 = 1.360 \pm 0.073,$ where the number after “ \pm ” is
 168 the standard deviation of the Gaussian fit. Using the peak frequencies of the three peaks,
 169 we find $\alpha = 1.1,$ a reasonable value based on previous studies [*Denton, 2006; Denton et al.,*
 170 *2006b*]. This value indicates that the mass density increases mildly as one moves from the
 171 magnetic equator (where LR_E/R in (1) equals unity) to higher magnetic latitude, MLAT
 172 (where the geocentric radius $R < LR_E$).

173 In order to get a measure of the possible spread in α based on the spread (standard
 174 deviation) of the observed frequency ratios, we do a Monte Carlo set of calculations with
 175 a random set of frequencies generated using probabilities consistent with the standard
 176 deviations of the frequencies. In other words, a large number of random choices would
 177 give for each peak a Gaussian distribution of frequencies with the same standard deviation.
 178 Using 1000 random combinations of the three frequencies, we find a median value of α of
 179 1.2, with the first quartile and third quartile values of -1.7 and 3.0, respectively. That is,
 180 one fourth of the 1000 α values were below -1.7, and one fourth were above 3.0. The mean
 181 and standard deviation values are 0.3 and 3.6, respectively. Note that the mean values
 182 are typically skewed toward negative values from the value based on the peak frequencies.
 183 This is because a Gaussian in the linear (rather than log) frequency is used, and negative
 184 changes in frequency have a larger effect on the results because they lead to a larger
 185 logarithmic or factor change in the frequency. The fundamental mode ($n = 1$), with small
 186 frequency, is especially sensitive to this effect, and decreased fundamental mode frequency

187 is correlated with peaked mass density at the magnetic equator, corresponding to negative
188 α .

189 Based on these numbers (standard deviation of 3.6), one might think that the value
190 of α is known very imprecisely. There are, however, two considerations that reduce the
191 strength of this conclusion. First of all, we are primarily interested in determining the
192 most common or typical field line distribution. The standard deviation of a mean is
193 reduced relative to the standard deviation of a set of measurements roughly by the square
194 root of the number of measurements. Using the number of frequencies measured in the
195 4th harmonic ($n = 4$, with the smallest number of measurements), equal to 58,400, we
196 estimate the standard deviation of the mean in α as $3.6/\sqrt{58400} = 0.015$, a very small
197 number.

198 But, as discussed by *Takahashi and Denton* [2007], there is reason to suspect that the
199 spread in α values corresponding to the real field line distribution of the magnetospheric
200 mass density at geostationary orbit is smaller than the spread of 3.6 consistent with the
201 observations. This is because the uncertainty in frequency ratio due to the uncertainty
202 of individual frequency measurements makes up a significant fraction of the total spread
203 in the frequency ratios. Thus the real spread in the precise frequency ratios and the
204 corresponding spread in α values are likely to be smaller.

205 For instance, assuming a resolution of 0.56 mHz due to a 30 min time window, we
206 use (2) to calculate the root mean squared error $\delta\bar{f}_n$ for the three harmonics $n = 1$,
207 2, and 4, and get 0.027, 0.026, and 0.043, respectively. Comparing to the standard
208 deviation of the Gaussian fits, 0.034, 0.037, and 0.073, we see that the relative errors due
209 to resolution account for a significant fraction of the uncertainty, especially for $n = 1$, and

210 2. Assuming that the measurement uncertainty due to resolution and the real uncertainty
 211 add in quadrature (square root of the sum of the squares), we estimate a real uncertainty
 212 of 0.022, 0.027, and 0.063 for $n = 1, 2,$ and $3,$ respectively. If we use these uncertainties
 213 for the frequency ratios, we find first quartile, median, and third quartile values of -1.0,
 214 1.0, and 2.3, respectively, or a mean value of α of 0.4 with standard deviation of 2.5. So
 215 the standard deviation in this case (2.5) is lower than that found using the total spread
 216 in the relative frequencies (3.5).

217 Below we will find α in three-dimensional bins with different combinations of MLT, AE,
 218 and F10.7. The standard deviation of the values of α in those bins is 1.0. Since there are
 219 roughly an equal number of frequencies in each of these bins, the uncertainty in α for all
 220 the data due to variation in MLT, AE, and F10.7 must also be about 1.0. Assuming again
 221 that uncertainties add in quadrature, the unexplained uncertainty in α would be roughly
 222 $\sqrt{(2.5)^2 - (1.0)^2} = 2.3.$

223 We will not do this detailed a calculation of uncertainty for the remaining results. But
 224 a reasonable spread in α around the values we calculate is probably something like 2.3.
 225 The mean values, however, are likely to be very close to the values that we find.

3. One Dimensional Modeling

226 Now for each of the three variables, MLT, F10.7, and AE, we divide our set of frequencies
 227 into 8 bins. We call this 1D binning. Values of F10.7 measured in solar flux units (sfu
 228 $= 10^{-22}\text{Wm}^{-2}\text{Hz}^{-1}$), and AE measured in nT, as well as solar wind parameters needed
 229 for the TS05 magnetic field model, are interpolated from hourly values from the National
 230 Aeronautics and Space Administration Goddard Space Flight Center OMNI data set
 231 through OMNIWeb [*King and Papitashvili, 2005*]. MLT is measured in h. The bin

232 divisions are determined using quantiles Q_i that extend to $i/8$ th of the data points, where
 233 i is an integer between 1 and 7, when those data points are ordered from lowest to
 234 highest. Thus each bin has one eighth of the frequencies. This method ensures that we
 235 have comparable statistics in each bin. Table 1 shows the quantile values for each of
 236 the three variables in addition to the minimum value (or Q_0 for 0/8th of the data) and
 237 maximum value (or Q_8 for 8/8th of the data). The boldface even numbered quantile
 238 values, which are quartiles, will be used in section 4 to divide the data into four bins.

239 Now for each of the three variables, and within each of the 8 bins, we fit Gaussians to
 240 the \bar{f}_1 , \bar{f}_2 , and \bar{f}_4 peaks. The distribution of frequencies and Gaussian fits are shown in
 241 Figure 2 for the first bin of MLT with $0.01 \text{ h} \leq \text{MLT} < 5.39 \text{ h}$. The data used for the
 242 Gaussian fits includes bins with a number of frequencies equal to at least half the peak
 243 value (black x symbols in Figure 2). Because some peaks were steep (especially for the 3D
 244 binning described in section 4), we added for each peak two additional points with exactly
 245 one half the peak value (black circles in Figure 2). These were obtained by interpolation
 246 using the values in adjacent bins. Then the best least-squares Gaussian fits were obtained
 247 for each peak (red curves in Figure 2). The data used for the fitting was limited to one
 248 half the peak value in order to avoid contamination by adjacent peaks (particularly for
 249 $n = 4$). The rest of the frequency distribution, while not used for the fits, is shown in
 250 Figure 2 as the dotted black curve.

251 Figure 3 shows the peak normalized frequency \bar{f}_n (black x symbols) for $n = 1$ (row
 252 A), $n = 2$ (row B), and $n = 4$ (row C) for the binned distributions of MLT (column a),
 253 F10.7 (column b), and AE (column c). The fact that there is variation in the frequency
 254 ratios with respect to MLT, F10.7, and AE, indicates that the field line distribution is

255 varying with respect to these parameters. Because there is some apparent noisiness in
 256 the values, we smooth the data. The values binned by F10.7 and AE are fit with a
 257 quadratic polynomial. We didn't feel that the polynomial fits with respect to MLT were
 258 as satisfactory, so in that case we smoothed the interior binned values y_i for bin i using
 259 $0.5y_i + 0.25(y_{i-1} + y_{i+1})$. The smoothed values are shown by the red curves in Figure 3.
 260 The standard deviation of the observed frequencies is shown by the error bars in Figure 3,
 261 and the spread of observed frequencies in the peaks (length of error bars) is larger than
 262 the variation of the peak frequencies (x symbols) with respect to the parameters on the
 263 horizontal axis of each panel. As was discussed in section 2, some of this spread is probably
 264 from the uncertainty due to the resolution in frequency. But even if this is factored out,
 265 the spread in observed frequencies is larger than the variation with respect to MLT, F10.7,
 266 or AE.

267 For each 1D bin, the wave equation is solved to find the value of α for which the
 268 theoretical frequencies best match the smoothed frequency ratios from Figure 3. The black
 269 open circles in Figure 4 show the results for variation with respect to MLT (Figure 4a),
 270 F10.7 (Figure 4b), and AE (Figure 4c). From this plot, we see that α decreases with
 271 respect to MLT (over the dayside range of MLT sampled) and F10.7, but increases with
 272 respect to AE. The strongest dependence is on MLT.

273 Using the Eureqa Formulize nonlinear genetic regression software [*Schmidt and Lipson,*
 274 2009] to find potential mathematical models for the F10.7 and AE dependence, and using
 275 a Fourier expansion for the MLT dependence up to the sine and cosine of twice the angle
 276 around the Earth, we chose the following analytical formulas:

$$\alpha_{1D\text{model,MLT}} = 1.1 + 1.4 \cos((\text{MLT} - 2.1) \cdot 15^\circ) + 0.3 \cos(2 \cdot (\text{MLT} - 2.8) \cdot 15^\circ), \quad (4)$$

$$\alpha_{1D_{\text{model},F10.7}} = 2.3 - \frac{49}{F10.7} - 0.0065 \cdot F10.7, \quad (5)$$

$$\alpha_{1D_{\text{model},AE}} = 0.8 + 0.00116AE. \quad (6)$$

277 These analytical formulas were chosen because they well fit the data points, are relatively
 278 simple, and are relatively well behaved over the full range of parameter values (from
 279 minimum to maximum) listed in Table 1. The weighted standard deviation of these
 280 formulas from the data points is less than 0.05 for each model, where the weights were the
 281 squared inverse of third quartile value of α minus the first quartile value for a distribution
 282 of 1000 frequencies consistent with the observed spread in frequencies. The red curves in
 283 Figure 4 show these formulas over these full ranges, (4) in Figure 4a, (5) in Figure 4b,
 284 and (6) in Figure 4c. Note that (4) in Figure 4a is periodic, and (5) in Figure 4b and (6)
 285 in Figure 4c vary linearly with respect to F10.7 and AE, respectively, at large values.

286 Based on the behavior of the data points, these were conservative choices and they
 287 lead to reasonable curves where extrapolated. One should, however, use caution when
 288 extrapolating. When far away from the range of data points in Figure 4, $4.2 \text{ h} \leq \text{MLT} \leq$
 289 16.2 h , $F10.7 \leq 218 \text{ sfu}$, and $AE \leq 603 \text{ nT}$, the formulas are without doubt questionable.

290 Again, a Monte Carlo simulation using the observed spread in frequencies leads to a
 291 large variation in the inferred α at the data points; the standard deviations for the points
 292 range between 3.3 and 4.2.

4. Three Dimensional Modeling

293 Now we want to divide the frequency data using simultaneous divisions with respect
 294 to all three parameters, MLT, F10.7, and AE. We call this 3D binning. In order to have
 295 adequate statistics in each bin, we use 4 bins for each variable, so that the total number

of bins is $4^3 = 64$. The boundaries for the bins for each parameter are the quartile values for each individual parameter. These are the bold values listed in Table 1. The mean values of each parameter in each of the four bins with respect to an individual parameter are listed in Table 2. Note that the mean values are between the quartile values listed in Table 1, as they must be. But the mean values are not necessarily near the center of each possible range. For instance, the mean MLT value in the first of four bins (5.1 h from Table 2) is close to the upper range of the first bin (6.69 h from Table 1), though this bin includes values ranging from 0.01 h to 6.69 h (Table 1). Similarly the mean in the 4th MLT bin (14.6 h) is close to the lower boundary of the 4th bin (11.9 h). This is because the distribution of toroidal Alfvén waves is strongly peaked on the dayside [Takahashi *et al.*, 2010]. Because of this, our mean bin values will be concentrated also on the dayside (ranging from MLT = 5.1 h to 14.6 h).

Note also that the number of frequencies in each 3D bin will not be exactly equal, as they were for the 1D bins, because the quartile values are chosen for each parameter using all the data. But the number of frequencies in the 3D bins typically vary by only about a factor of 2.

Figure 5 shows the distribution of frequencies for the 3D bin with the lowest values of MLT, F10.7, and AE in the same format as Figure 2. The ranges of the parameters for this bin extend up to the lowest bold numbers listed in Table 1 and are also indicated in the figure. The red curves in the figure show the Gaussian fits to the peaks. The frequency distribution is definitely more noisy here than was the case of Figure 2. This is because the 3D bins contain roughly $1/64$ of the data, whereas the 1D bins contained $1/8$

318 of the data. Nevertheless, we consider the data adequate to find the three peaks. And we
 319 verified that all 64 sets of peaks were of similar quality.

320 The Alfvén wave equation is solved for each of the 64 sets of frequency ratios corre-
 321 sponding to the 64 3D bins. The values of α based on the peak frequencies for each bin
 322 vary between -1.1 and 2.9. For each set of ratios, we vary α until the calculated frequency
 323 ratios best matches the binned ratios in a least-squares sense. Then using linear regres-
 324 sion with some guidance from Eureka Formulize, we find the following model for the 3D
 325 α values as a function of MLT, F10.7, and AE.

$$\begin{aligned} \alpha_{3D\text{model}} = & 2.2 + 1.3 \cdot \cos(\text{MLT} \cdot 15^\circ) \\ & + 0.0026 \cdot \text{AE} \cdot \cos((\text{MLT} - 0.8) \cdot 15^\circ) \\ & + 2.1 \cdot 10^{-5} \cdot \text{AE} \cdot \text{F10.7} - 0.010 \cdot \text{F10.7}, \end{aligned} \quad (7)$$

326 where MLT is in h, AE is in nT, and F10.7 is in sfu. To get this formula, we minimize the
 327 weighted standard deviation in the α values calculated using the peak frequencies, using
 328 weights equal to the squared inverse of the difference in the third quartile α value and the
 329 first quartile value using 1000 random frequencies for each bin. This formula fits the 3D
 330 α values within a weighted standard deviation of 0.3. The weighted standard deviation
 331 of the data in the bins was 1.0 around a weighted average of 1.1. So (7) accounts for
 332 about 90% of the squared variation (proportional to the standard deviation squared) in
 333 the binned values.

334 The 3D bin values of MLT, F10.7, and AE are close to, but not exactly the same, as
 335 the values listed in Table 2. For the purpose of plotting only, we adjust the 3D α values

336 using the following formula

$$\alpha_{i,j,k}^{\text{adjusted}} = \alpha_{i,j,k}^{\text{original}} + \alpha_{3\text{Dmodel}}(\text{MLT}_i, \text{F10.7}_j, \text{AE}_k) - \alpha_{3\text{Dmodel}}(\text{MLT}_{i,j,k}, \text{F10.7}_{i,j,k}, \text{AE}_{i,j,k}) \quad (8)$$

337 where MLT_i , F10.7_j , and AE_k are the 1D bin values listed in Table 2, and $\text{MLT}_{i,j,k}$,
 338 $\text{F10.7}_{i,j,k}$, and $\text{AE}_{i,j,k}$ are the mean parameter values in the 3D bins for the i th MLT bin,
 339 the j th F10.7 bin, and the k th AE bin. With this adjustment, we hope to be able to
 340 see the variation in one of the three parameters keeping the other parameters constant.
 341 Most of the adjustments are small. The average adjustment is 0.02, showing that the
 342 adjustments do not significantly change the α values on average. The average absolute
 343 value of the adjustments is 0.07. The largest absolute value of the adjustment is 0.40.
 344 The largest part of this largest adjustment is due to a difference in the 3D bin value of
 345 AE from the 1D value, but the difference in MLT also contributes. In any case, all of
 346 these adjustments are relatively small compared to the variation over the 3D bins (from
 347 -1.1 to 2.9).

348 Figure 6 shows line plots of α^{adjusted} versus AE for the various combinations of MLT and
 349 F10.7. For the most part, α^{adjusted} decreases with respect to increasing MLT, as indicated
 350 by the fact that for most data points the α^{adjusted} values are highest for the thick solid
 351 curves and lowest for the dotted curves. There are some exceptions. For instance, the
 352 rightmost data point on the dotted red curve, corresponding to the highest values of
 353 AE, MLT, and F10.7 may be an outlier. Again, for the most part, α^{adjusted} decreases
 354 with respect to increasing F10.7, as indicated by the fact that the curves with red color
 355 tend to be the lowest, while the curves with black color tends to be the highest. The
 356 AE dependence is more complicated. At $\text{MLT} = 5.1$ h (thick curves), α^{adjusted} tends to

357 increase with respect to AE. But at the latest local times, $MLT = 10.3$ h and 14.6 h
 358 (dashed and dotted curves), α^{adjusted} increases with respect to AE only at large F10.7 (red
 359 curves).

360 These trends can be seen in (7). The cosine function with MLT as an argument peaks
 361 near $MLT = 0$ h, which is significantly closer to the first bin value of $MLT = 5.1$ h than
 362 to the last bin value of $MLT = 14.6$ h. Therefore, $\alpha_{3D\text{model}}$ decreases with respect to
 363 MLT over the four MLT bin values. And $\alpha_{3D\text{model}}$ has a negative term with F10.7, so
 364 $\alpha_{3D\text{model}}$ generally decreases with respect to F10.7. Runs of Eureka Formulize indicated
 365 that the most important terms with AE were terms that combined AE with MLT or F10.7
 366 dependence. In fact, (7) does not have a simple linear term involving AE. The AE terms
 367 in $\alpha_{3D\text{model}}$ are multiplied by a cosine function in MLT that peaks near $MLT = 0$ h or
 368 by F10.7. So $\alpha_{3D\text{model}}$ increases with respect to AE mainly at MLT near 0 h or at large
 369 F10.7.

370 Figure 7 also shows α_{adjusted} in the 3D bins of the space of ($MLT, F10.7, AE$) (column
 371 a), as well as α_{model} (column b), and the difference $\alpha_{\text{model}} - \alpha_{\text{adjusted}}$ (column c). Again, α
 372 becomes more negative (indicated in Figure 7a and b by more bluish color) with respect
 373 to increasing MLT (over the dayside range of MLT values used here) and with increasing
 374 F10.7. We indicate in Figure 7 the bins for which the AE dependence makes a difference
 375 of at least 0.4 with green circles. If the AE dependence is positive, the circles are filled
 376 with red color, whereas if the AE dependence is negative, the circles are filled with blue
 377 color. (The circles around the blue color may appear cyan due to their proximity to
 378 the blue color.) The actual AE dependent terms in (7) are dominantly positive for the
 379 dayside range of MLT shown in Figure 7, but in order to show the effect of including

380 the AE dependence, we generated a second model without the AE dependent terms,
 381 $\alpha_{\text{modelMinusAE}} \equiv 2.1 + 1.8 \cos((\text{MLT} - 0.5) \cdot 15^\circ) - 0.0047 \text{ F10.7}$, and subtracted the value
 382 of $\alpha_{\text{modelMinusAE}}$ from α_{model} calculated using (7). With this procedure, we find that $\alpha_{\text{model}} -$
 383 $\alpha_{\text{modelMinusAE}}$ is negative at small AE. The AE dependence is important for MLT close to
 384 0 h and for large F10.7, as was described in reference to Figure 6, and these dependencies
 385 explain the pattern of green circles in Figure 7.

386 Finally, as suggested by the weighted standard deviations mentioned above (0.3 for the
 387 difference between model and data versus 1.0 for the data itself), Figure 7 shows that the
 388 difference $\alpha_{\text{model}} - \alpha_{\text{adjusted}}$ is much less than the variation in α_{adjusted} over the 3D space,
 389 indicating that the model is doing a good job representing most of the variation of α in
 390 Figure 7. Once again, the standard deviation of the α values consistent with the observed
 391 spread in the frequencies is large, between 2.9 and 4.4 in the 64 bins. Such spreads are
 392 somewhat larger than the variation of α in the bins which is shown in Figure 7. Therefore
 393 there may be a significant variation of α values around that of α_{model} , but α_{model} should
 394 well predict the typical α values.

395 While (7) is a reasonable formula for most of the possible range of parameters, the terms
 396 proportional to AE and F10.7, and especially the one proportional to both, can get very
 397 large for large values of AE and F10.7. So we do not consider (7) to be a good model for
 398 the full range of possible parameters. One possible way to handle this problem would be
 399 to limit the range of $\alpha_{3\text{Dmodel}}$ to values between -2 and +4. These limits are close to the
 400 limits of α in Figure 6.

5. Discussion

401 Early theoretical calculations by *Angerami and Carpenter* [1966] suggested that realistic
402 values of α might range between 0.5 or 1 and 4. *Takahashi and Denton* [2007] found that
403 α tends to be more negative at afternoon MLT values. This result is consistent with
404 our current findings. *Denton et al.* [2006b, and references therein], using data from the
405 CRRES spacecraft, found that α appeared to be negative, suggesting a local peak in
406 mass density at the magnetic equator. They investigated the relation of this local peak
407 to geomagnetic activity, using the Kp and Dst indices. We found that there is a higher
408 correlation with AE (not shown), and have used that in our model. Whereas *Denton et al.*
409 [2006b] found more negative α correlated with increased geomagnetic activity as indicated
410 by Kp or negative Dst, we find more positive α correlated with increased geomagnetic
411 activity as indicated by larger AE.

412 Ideally, we would now explain all the dependencies that we see. Unfortunately, we are
413 not able to do that. But we can make some observations and speculations. The midnight
414 to dusk plasma at geostationary orbit is often on magnetic flux tubes that drift on open
415 $\mathbf{E} \times \mathbf{B}$ drift paths eastward from the magnetotail on the nightside to the magnetopause on
416 the dayside. A predominantly cold or warm population called the plasma cloak gradually
417 fills these flux tubes through upflow from the ionosphere as they travel on these trajectories
418 [*Chappell et al.*, 2008; *Lee and Angelopoulos*, 2014]. At dawn local time, this population
419 of particles tends to be moving up the field line (particles have a field aligned pitch angle
420 distribution). Therefore it is certainly possible that the density of particles would be
421 higher at high magnetic latitudes closer to the source of the population at low altitude,
422 and thus correspond to large positive values of α . As this population drifts around the

423 dayside magnetosphere toward dusk, it may gradually refill at the magnetic equator and
424 become more trapped. A highly trapped (90° pitch angle population) would be peaked
425 at the magnetic equator so that negative α would be appropriate. Another possible
426 reason for more negative α at dusk is that there is at that location a greater contribution
427 to the mass density from trapped ring current particles (with 10s of keV temperature),
428 especially O^+ , that drift westward (because of the westward ∇B and curvature drifts)
429 from the magnetotail.

430 Negative values of α occur at large F10.7, for which we expect a larger concentration
431 of O^+ [*Denton et al.*, 2011]. Perhaps the O^+ becomes more trapped than the H^+ for
432 reasons we don't currently understand. Perhaps the centrifugal force due to the rotational
433 motion around the Earth creates a pseudo-potential that preferentially traps the O^+ or
434 perhaps the O^+ is heated in the perpendicular direction by the Alfvén waves themselves
435 [*Denton et al.*, 2006a] or by electromagnetic ion cyclotron (EMIC) or other waves. Or
436 perhaps the detailed wave particle interactions that lead to trapping favor the trapping
437 of high mass particles.

438 Greater activity as indicated by larger AE might correspond to greater upflow of new
439 particles in the plasma cloak, so that more positive α may be appropriate. The effect
440 of greater AE on α would be concentrated in the predawn local time sector where the
441 plasma in the cloak starts to flow up the field lines that are $\mathbf{E} \times \mathbf{B}$ drifting eastward from
442 the nightside.

443 These factors relate at least somewhat to the buildup of mass near the magnetic equator.
444 We mentioned that equatorial refilling may occur as the local time changes from dawn to
445 dusk [*McComas et al.*, 1993; *Menk et al.*, 1999; *Galvan et al.*, 2008] and that there might

446 be refilling from the ionosphere on the nightside correlated with AE. We stated that
 447 there is more O+ and therefore larger mass density at solar maximum, corresponding to
 448 larger F10.7. The question arises as to whether the α values are primarily related to the
 449 value of the equatorial mass density itself. Clearly, if the mass density is very low at
 450 the magnetic equator, it must eventually increase rapidly with respect to MLAT so as to
 451 reach ionospheric values; that is, α should be large.

452 In order to investigate the correlation of α with the equatorial mass density, we find the
 453 log average value of ρ_m in the 64 3-D bins in order to model the variation of α in these
 454 bins with ρ_m alone. First we solve for the equatorial mass density for each point in our
 455 data set. As mentioned in the Introduction, the inferred equatorial mass density depends
 456 on the value of α that is assumed. We used a formula for α that was very close to that of
 457 (7). (Equation (7) has been slightly modified since we calculated the mass densities due
 458 to slight modifications in our method, but the difference would have only a slight effect
 459 on the inferred equatorial mass density.) If we model ρ_m with the same functional form
 460 used for (7), we find

$$\begin{aligned} \log_{10}(\rho_m) = & 0.46 - 0.17 \cdot \cos((\text{MLT} - 3.7) \cdot 15^\circ) \\ & - 0.00022 \cdot \text{AE} \cdot \cos((\text{MLT} - 23.3) \cdot 15^\circ) \\ & - 1.7 \cdot 10^{-6} \cdot \text{AE} \cdot \text{F10.7} + 0.0042 \cdot \text{F10.7} \end{aligned} \quad (9)$$

461 with a weighted standard deviation of 0.19 (a factor of 1.5). For each measured frequency,
 462 a set of 64 frequencies was generated consistent with the uncertainty in the frequency. For
 463 the determination of (9), the median value of ρ_m was used for each data point with a weight
 464 equal to the inverse difference between the first and third quartile. Comparing (9) to (7),
 465 we see that term by term, increased ρ_m correlates with decreased α .

To see how well we can predict α using ρ_m alone, we now calculate the log average of ρ_m in the 64 3D bins (divided using ranges of MLT, F10.7, and AE as before). For these 64 bins, we model α with a simple formula suggested by Eureka Formulize as

$$\alpha_{\rho_m} = 3.3 - 2.87 \log_{10}(\rho_m). \quad (10)$$

466 Here we used weights equal to the inverse of the uncertainty in the mean value of $\log_{10}(\rho_m)$.
 467 The weighted standard deviation of α_{ρ_m} from α_{original} was 0.7, significantly lower than 1.0,
 468 the standard deviation of α_{original} with respect to its mean value, but significantly larger
 469 than 0.3, the standard difference between $\alpha_{3\text{Dmodel}}$ and α_{original} . To put it another way,
 470 the mass density dependence in (10) accounts for about half the reduction in variance
 471 (proportional to the standard deviation squared) going from a mean value to $\alpha_{3\text{Dmodel}}$.

472 Figure 8 shows the adjusted α values, α_{adjusted} , and α_{ρ_m} values (also adjusted) in the
 473 same format as Figure 7. Figure 8b shows some of the same trends as Figure 8a, but the
 474 agreement with α_{ρ_m} is worse than that of $\alpha_{3\text{Dmodel}}$ in Figure 7b.

475 *Takahashi et al.* [2004] found evidence for α varying with the electron density n_e . For
 476 high n_e (“plasmasphere”) plasma, they showed that the harmonic frequencies were consis-
 477 tent with a monotonic ρ_m dependence. The dependence for the low n_e (“plasmatrrough”)
 478 plasma was probably not consistent with a monotonic dependence. But using the power
 479 law form, as we do in this paper, the best fitting α value appeared to be more negative
 480 for low n_e . On the face of it, this dependence appears to be the opposite of what we find
 481 in (10), which indicates that α decreases with respect to ρ_m . However, we must keep in
 482 mind that the CRRES data used by Takahashi et al. were measured at solar maximum.
 483 And at solar maximum, there is a large contribution from O+ to the mass density in the
 484 plasmatrrough [*Denton et al.*, 2011]. Thus during solar maximum, there may be no good

485 correlation between n_e and ρ_m . We are unable to explore the relation between α and n_e
486 using data from GOES, since GOES did not measure n_e .

487 Despite our lack of complete theoretical understanding, we have found an empirical
488 model for α , equation (7), that well fits the observations, at least in an average sense.
489 This should be useful for future calculations of the frequency and field line structure of
490 toroidal Alfvén waves and for modeling other MHD wave phenomena.

491 **Acknowledgments.** Work at Dartmouth was supported by NSF grant AGS-1105790
492 and NASA grants NNX10AQ60G and NNG05GJ70G. Work at JHU APL was supported
493 by NSF Grant AGS-1106427. Values of AE come originally from the World Data Center
494 for Geomagnetism at Kyoto University, and values of F10.7 come originally from NOAA's
495 National Geophysical Data Center. Numerical data shown in this paper is available from
496 the lead author upon request.

References

- 497 Angerami, J. J., and D. Carpenter (1966), Whistler studies of the plasmopause in the
498 magnetosphere. 2. Electron density and total tube electron content near the knee in
499 magnetospheric ionization, *Journal of Geophysical Research*, *71*(3), 711.
- 500 Chappell, C. R., M. M. Huddleston, T. E. Moore, B. L. Giles, and D. C. Delcourt (2008),
501 Observations of the warm plasma cloak and an explanation of its formation in the
502 magnetosphere, *J. Geophys. Res.*, *113*(A9), a09206, doi:10.1029/2007ja012945.
- 503 Denton, M. H., J. E. Borovsky, R. M. Skoug, M. F. Thomsen, B. Lavraud, M. G. Hen-
504 derson, R. L. McPherron, J. C. Zhang, and M. W. Liemohn (2006a), Geomagnetic
505 storms driven by ICME- and CIR-dominated solar wind, *J. Geophys. Res.*, *111*(A7),

506 doi:10.1029/2005JA011436.

507 Denton, R. E. (2006), Magneto-seismology using spacecraft observations, in *Magneto-*
508 *spheric ULF waves: Synthesis and new directions*, edited by K. Takahashi, P. J. Chi,
509 R. E. Denton, and R. L. Lysak, Geophysical monograph, pp. 307–317, American Geo-
510 physical Union, Washington, DC, english.

511 Denton, R. E., and D. L. Gallagher (2000), Determining the mass density along magnetic
512 field lines from toroidal eigenfrequencies, *J. Geophys. Res.*, *105*(A12), 27,717–27,725.

513 Denton, R. E., M. R. Lessard, R. Anderson, E. G. Miftakhova, and J. W. Hughes (2001),
514 Determining the mass density along magnetic field lines from toroidal eigenfrequencies:
515 Polynomial expansion applied to CRRES data, *J. Geophys. Res.*, *106*(A12).

516 Denton, R. E., K. Takahashi, R. R. Anderson, and M. P. Wuest (2004), Magnetospheric
517 toroidal Alfvén wave harmonics and the field line distribution of mass density, *J. Geo-*
518 *phys. Res.*, *109*(A6), A06202, doi:10.1029/2003JA010201.

519 Denton, R. E., K. Takahashi, I. A. Galkin, P. A. Nsumei, X. Huang, B. W. Reinisch, R. R.
520 Anderson, M. K. Sleeper, and W. J. Hughes (2006b), Distribution of density along mag-
521 netospheric field lines, *J. Geophys. Res.*, *111*(A4), A04213, doi:10.1029/2005JA011414.

522 Denton, R. E., P. Decreau, M. J. Engebretson, F. Darrouzet, J. L. Posch, C. Mouikis,
523 L. M. Kistler, C. A. Cattell, K. Takahashi, S. Schaefer, and J. Goldstein (2009), Field
524 line distribution of density at L=4.8 inferred from observations by CLUSTER, *Ann.*
525 *Geophys.*, *27*(2), 705–724.

526 Denton, R. E., M. F. Thomsen, K. Takahashi, R. R. Anderson, and H. J. Singer (2011),
527 Solar cycle dependence of bulk ion composition at geosynchronous orbit, *J. Geophys.*
528 *Res.*, *116*, a03212, doi:10.1029/2010ja016027.

- 529 Galvan, D. A., M. B. Moldwin, and B. R. Sandel (2008), Diurnal variation in plasma-
530 spheric He(+) inferred from extreme ultraviolet images, *J. Geophys. Res.*, *113*(A9),
531 a09216, doi:10.1029/2007ja013013.
- 532 King, J. H., and N. E. Papitashvili (2005), Solar wind spatial scales in and comparisons
533 of hourly wind and ace plasma and magnetic field data, *J. Geophys. Res.*, *110*(A2),
534 a02104, doi:10.1029/2004ja010649.
- 535 Kress, B. T., M. K. Hudson, M. D. Looper, J. Albert, J. G. Lyon, and C. C.
536 Goodrich (2007), Global MHD test particle simulations of >10 MeV radiation belt
537 electrons during storm sudden commencement, *J. Geophys. Res.*, pp. A09,215–1–11,
538 doi:10.1029/2006ja012218.
- 539 Kwon, H. J., K. H. Kim, D. H. Lee, K. Takahashi, V. Angelopoulos, E. Lee, H. Jin,
540 Y. D. Park, J. Lee, P. R. Sutcliffe, and H. U. Auster (2012), Local time-dependent Pi2
541 frequencies confirmed by simultaneous observations from THEMIS probes in the inner
542 magnetosphere and at low-latitude ground stations, *J. Geophys. Res.*, *117*, a01206,
543 doi:10.1029/2011ja016815.
- 544 Lee, J. H., and V. Angelopoulos (2014), On the presence and properties of cold ions
545 near earth's equatorial magnetosphere, *J. Geophys. Res.*, *119*(3), 1749–1770, doi:
546 10.1002/2013ja019305.
- 547 Lyons, L. (1991), *A Practical Guide to Data Analysis for Physical Science Students*, Cam-
548 bridge University Press, Cambridge.
- 549 McComas, D. J., S. J. Bame, B. L. Barraclough, J. R. Donart, R. C. Elphic, J. T. Gosling,
550 M. B. Moldwin, K. R. Moore, and M. F. Thomsen (1993), Magnetospheric plasma
551 analyzer - Initial 3-spacecraft observations from geosynchronous orbit, *J. Geophys. Res.*,

- 552 98(A8), 13,453–13,465.
- 553 Menk, F. W., D. Orr, M. A. Clilverd, A. J. Smith, C. L. Waters, D. K. Milling, and B. J.
554 Fraser (1999), Monitoring spatial and temporal variations in the dayside plasmasphere
555 using geomagnetic field line resonances, *J. Geophys. Res.*, 104(A9), 19,955–19,969, doi:
556 10.1029/1999ja900205.
- 557 Perry, K. L., M. K. Hudson, and S. R. Elkington (2005), Incorporating spectral charac-
558 teristics of Pc5 waves into three- dimensional radiation belt modeling and the diffusion
559 of relativistic electrons, *J. Geophys. Res.*, 110(A3), a03215, doi:10.1029/2004ja010760.
- 560 Press, W. H., B. P. Flannery, S. A. Teukolsky, and W. T. Vetterling (1986), *Numerical*
561 *Recipes*, Cambridge Univ. Press, New York.
- 562 Price, I. A., C. L. Waters, F. W. Menk, G. J. Bailey, and B. J. Fraser (1999), A technique to
563 investigate plasma mass density in the topside ionosphere using ULF waves, *J. Geophys.*
564 *Res.*, 104(A6).
- 565 Schmidt, M., and H. Lipson (2009), Distilling free-form natural laws from experimental
566 data, *Science*, 324(5923), 81–85, doi:10.1126/science.1165893.
- 567 Schulz, M. (1996), Eigenfrequencies of geomagnetic field lines and implications for plasma-
568 density modeling, *J. Geophys. Res.*, 101(A8), 17,385–17,397, doi:10.1029/95ja03727.
- 569 Singer, H. J., D. J. Southwood, R. J. Walker, and M. G. Kivelson (1981), Alfvén-wave
570 resonances in a realistic magnetospheric magnetic-field geometry, *J. Geophys. Res.*,
571 86(NA6).
- 572 Takahashi, K., and R. E. Denton (2007), Magnetospheric seismology using multiharmonic
573 toroidal waves observed at geosynchronous orbit, *J. Geophys. Res.*, 112(A5), A05204,
574 doi:10.1029/2006JA011709.

- 575 Takahashi, K., and R. L. McPherron (1982), Harmonic structure of pc 3-4 pulsations, *J.*
576 *Geophys. Res.*, *87*(NA3), 1504–1516.
- 577 Takahashi, K., R. E. Denton, R. R. Anderson, and W. J. Hughes (2004), Frequencies
578 of standing Alfvén wave harmonics and their implication for plasma mass distribution
579 along geomagnetic field lines: Statistical analysis of CRRES data, *J. Geophys. Res.*,
580 *109*(A8), A08202, doi:10.1029/2003JA010345.
- 581 Takahashi, K., R. E. Denton, and H. J. Singer (2010), Solar cycle variation of geosyn-
582 chronous plasma mass density derived from the frequency of standing Alfvén waves, *J.*
583 *Geophys. Res.*, *115*, doi:10.1029/2009ja015243.
- 584 Takahashi, K., R. E. Denton, W. Kurth, C. Kletzing, J. Wygant, J. Bonnell, L. Dai,
585 K. Min, C. W. Smith, and R. MacDowall (2014), Externally driven plasmaspheric ULF
586 waves observed by the Van Allen Probes, *J. Geophys. Res.*, *119*.
- 587 Tsyganenko, N. A., and M. I. Sitnov (2005), Modeling the dynamics of the inner
588 magnetosphere during strong geomagnetic storms, *J. Geophys. Res.*, *110*(A3), doi:
589 10.1029/2004ja010798.
- 590 Waters, C. L., F. W. Menk, M. F. Thomsen, C. Foster, and F. R. Fenrich (2006), Remote-
591 sensing the magnetosphere using ground-based observations of ULF waves, in *Magne-*
592 *tospheric ULF Waves: Synthesis and New Directions*, edited by K. Takahashi, P. J.
593 Chi, R. E. Denton, and R. L. Lysak, Geophysical Monograph, pp. 319–340, American
594 Geophysical Union, Washington D.C.

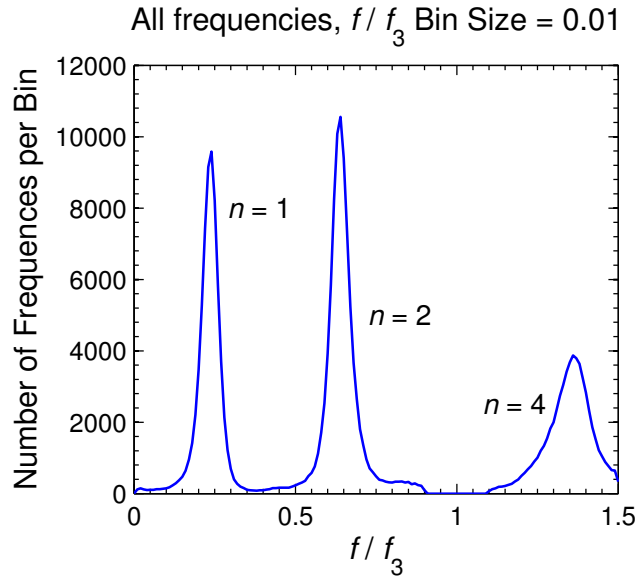


Figure 1. Distribution of normalized frequencies $\bar{f} \equiv f/f_3$ for the entire data set used in this paper. The bin size for \bar{f} is 0.01.

Table 1. Minimum, 8 Bin Quantile Divisions Q_i , and Maximum Values for Parameters

MLT, F10.7, and AE

Parameter	Min	Q_1	Q_2^a	Q_3	Q_4^a	Q_5	Q_6^a	Q_7	Max
MLT (h)	0.01	5.39	6.69	7.80	8.93	10.22	11.91	14.20	23.99
F10.7 (sfu)	65.9	70.1	73.7	80.5	94.4	115.8	144.6	184.7	346.5
AE (nT)	10.2	58.6	88.2	126.8	175.1	234.6	315.8	446.8	1794.

^a The boldface Q_i values are used in section 4 to divide the data into four bins.

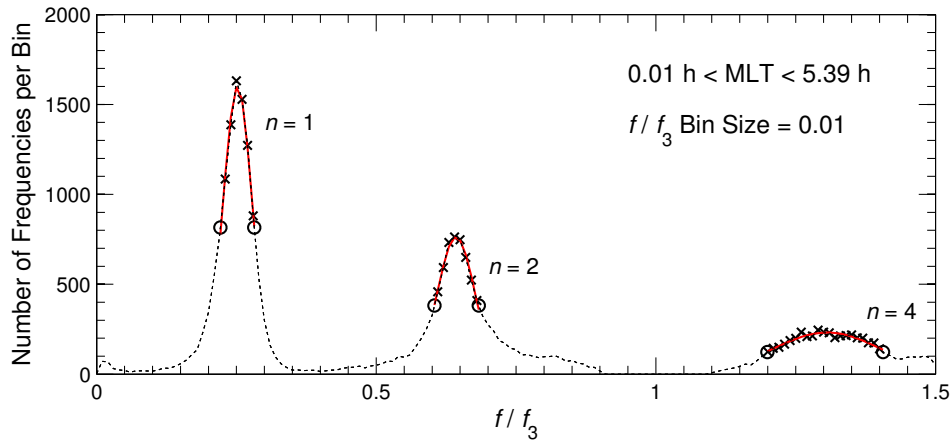


Figure 2. Distribution of frequencies \bar{f} in the three peaks (black x symbols) for the 1D bin with the lowest values of MLT ($0.01 \text{ h} \leq \text{MLT} < 5.39 \text{ h}$). The red curves are Gaussian fits to the peaks.

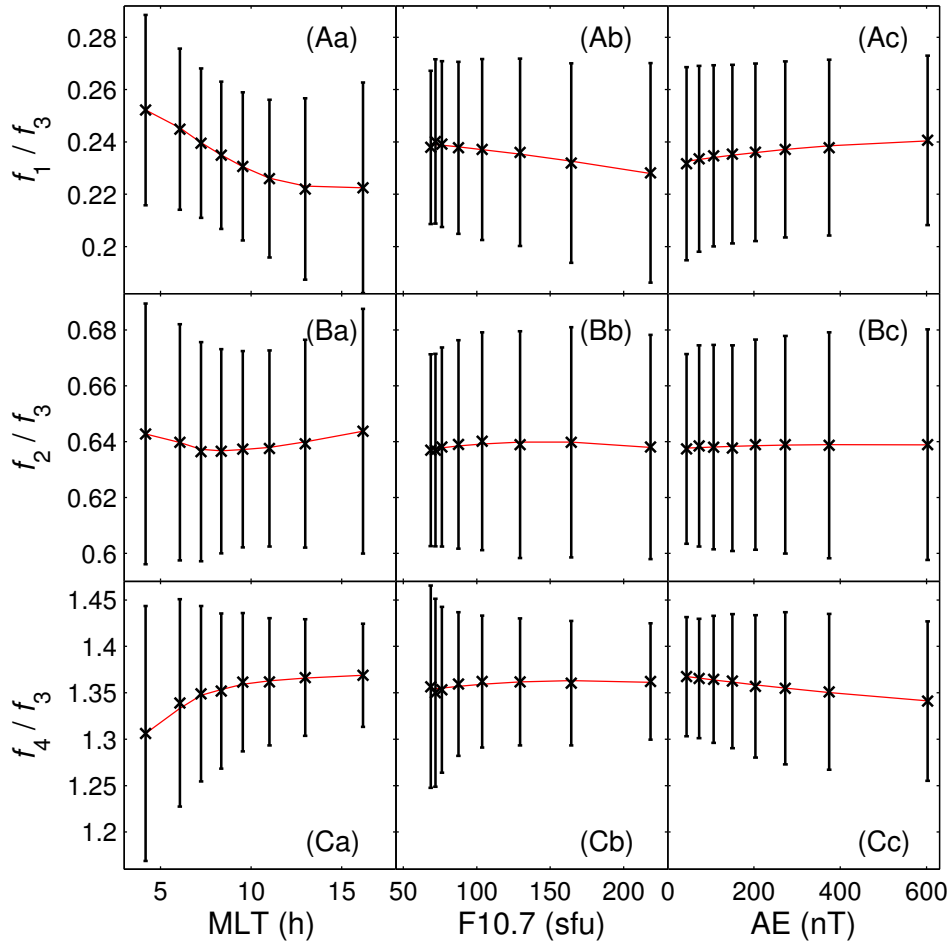


Figure 3. Peak normalized frequency $\bar{f}_n \equiv f_n/f_3$ for $n = 1$ (row A), $n = 2$ (row B), and $n = 4$ (row C) versus MLT (column a), F10.7 (column b), and AE (column c). The values from the fits in each bin are the black x symbols and the red curves are the values smoothed as described in the text.

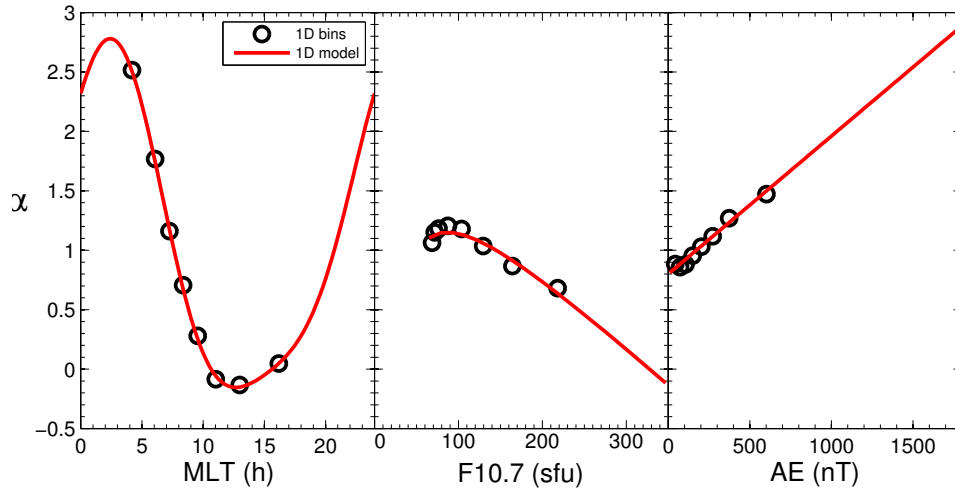


Figure 4. Values of the power law coefficient α versus (a) MLT, (b) F10.7, and (c) AE. The black circles are the values of α calculated using the 1D binned frequency ratios in Figure 3. The red curves are the analytical models (4–6) described in the text.

Table 2. Mean Values of Parameters MLT, F10.7, and AE, in 4 Bins Divided Using the Individual Parameters

Parameter	Bin 1	Bin 2	Bin 3	Bin 4
MLT (h)	5.1	7.8	10.3	14.6
F10.7 (sfu)	70.	82.	117.	191.
AE (nT)	58.	128.	238.	488.

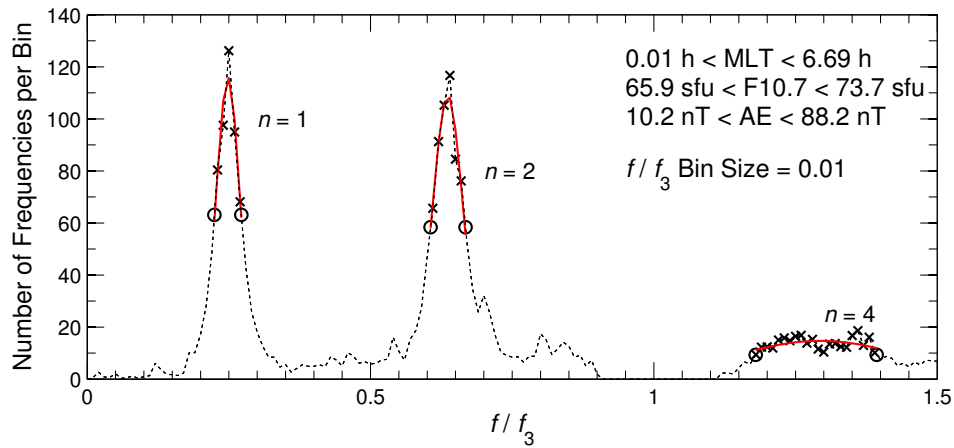


Figure 5. Like Figure 2, but for the 3D bin with the lowest values of MLT, F10.7, and AE. The ranges are listed in the panel.

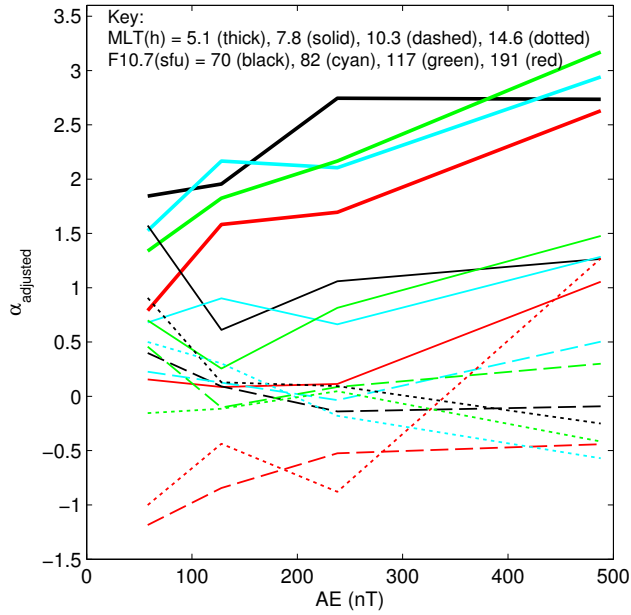


Figure 6. Values of $\alpha_{adjusted}$ versus AE for the 3D data. The curves vary in color corresponding to F10.7 values, and they vary in line style corresponding to MLT values, as indicated in the key. Higher F10.7 values are indicated by colors that are more red, and higher MLT values are indicated by line styles that are less weighty in appearance. (The thin dotted curve is the least weighty, while the thick solid curve is the most weighty.) In the key, “thick” indicates the thick solid curves, and “solid” indicates the thin solid curves.

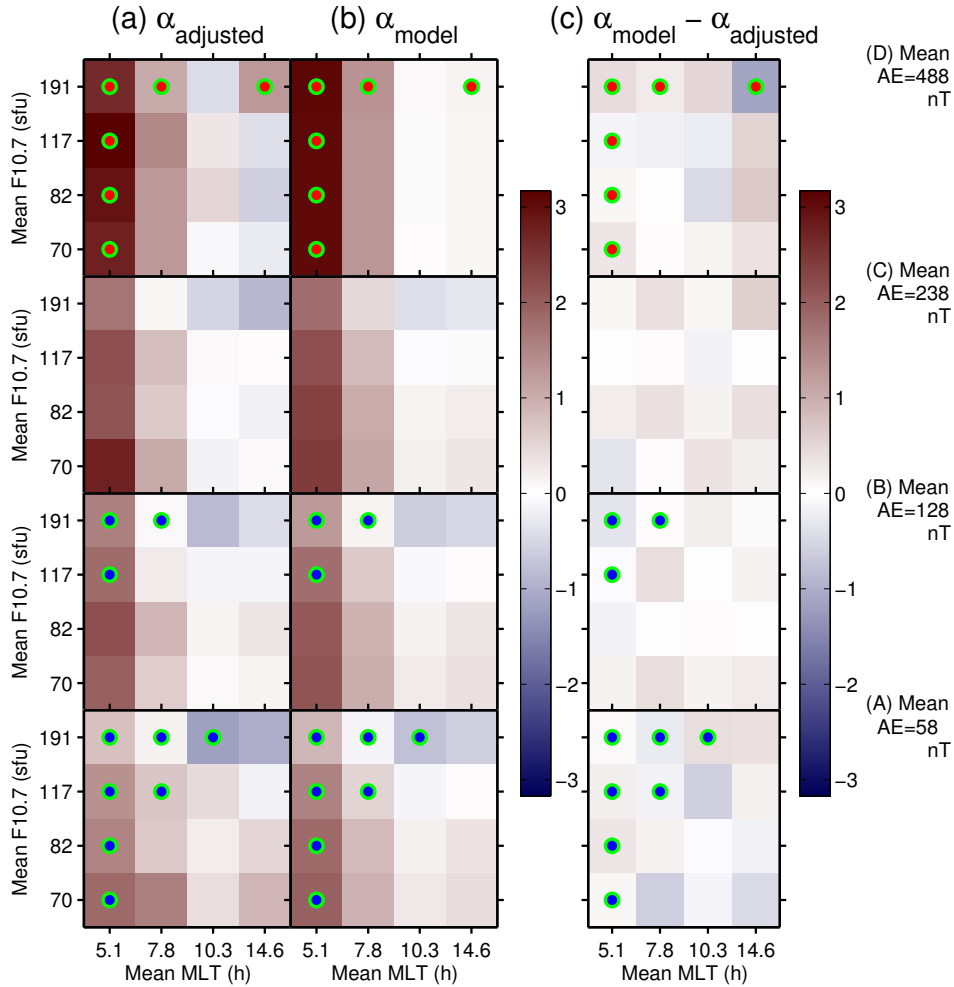


Figure 7. (a) Adjusted α values, α_{adjusted} , in the 3D bins, (b) model values, α_{model} , found using (7), and (c) $\alpha_{\text{model}} - \alpha_{\text{adjusted}}$, for (A) AE = 58 (bottom row or panels), (B) AE = 128, (C) AE = 238, and (D) AE = 488. In each panel, the values of α are shown using the blue to red color scale (at right) versus MLT on the horizontal axis and F10.7 on the vertical axis. The green circles (some of which may appear to be cyan) are points where the AE dependence led to a change in α_{model} of at least 0.4 as described in the text.

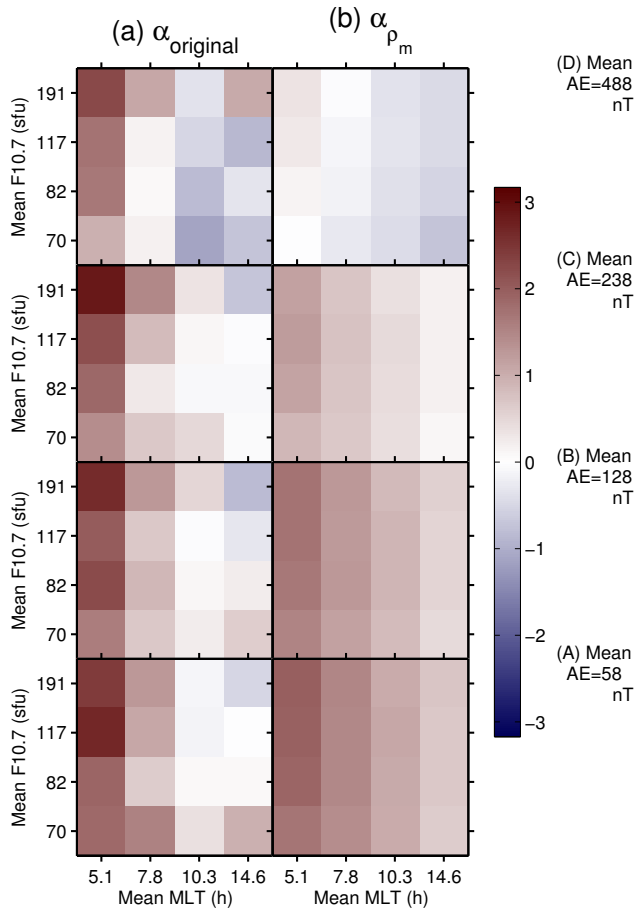


Figure 8. (a) Adjusted α values, α_{adjusted} , in the 3D bins, and (b) model values α_{ρ_m} using (10), for (A) AE = 58 (bottom row of panels), (B) AE = 128, (C) AE = 238, and (D) AE = 488. In each panel, the values of α are shown using the blue to red color scale (at right) versus MLT on the horizontal axis and F10.7 on the vertical axis.